 CMC, vol.2, no.4, pp.251-265, 2005

The Method of Fundamental Solutions Applied to the Calculation of Eigenfrequencies and Eigenmodes of 2D Simply Connected Shapes

Carlos J. S. Alves and Pedro R. S. Antunes [1]

Abstract: In this work we show the application of the Method of Fundamental Solutions (MFS) in the determination of eigenfrequencies and eigenmodes associated to wave scattering problems. This meshless method was already applied to simple geometry domains with Dirichlet boundary conditions (cf. Karageorghis (2001)) and to multiply connected domains (cf. Chen, Chang, Chen, and Chen (2005)). Here we show that a particular choice of point-sources can lead to very good results for a fairly general type of domains. Simulations with Neumann boundary condition are also considered.

keyword: Eigenfrequencies, Eigenmodes, Acoustic waves, Method of fundamental solutions

1 Introduction

The determination of the eigenvalues and eigenfunctions associated to the Laplace-Dirichlet operator in a bounded domain Ω is a well known problem with applications in acoustics (e.g. Courant and Hilbert (1953), Cox and Uhlig (2003)). For simple shapes, such as rectangles or circles in 2D, this leads to straightforward computations, without the need of a numerical algorithm. However, when the shape is non trivial, that computation requires the use of a numerical method. A standard finite differences method can produce good results when dealing with a particular type of shapes defined on rectangular grids, while for other type of shapes the finite element method or the boundary element method are appropriate (e.g. De Mey (1976)). These classical methods require extra computational effort; in one case, the construction of the mesh and the associated stiffness matrix, and in the other, the integration of weakly singular kernels. Here we propose a meshless method for solving the eigenvalue problem using the method of fundamental solutions (MFS). The MFS is a meshless method for linear PDEs with constant coefficients that falls in a general class of approaches called Trefftz methods. It has been mainly applied to boundary problems in PDEs, starting in the 1960s (e.g. Kupradze and Aleksidze (1964) or Arantes e Oliveira (1968)). The boundary conditions are usually imposed with collocation techniques, but other possibilities can be explored using Meshless Local Petrov-Galerkin schemes, as detailed in Atluri (2004). An account of the development can be found in Golberg and Chen (1996). The application of the MFS to the calculation of the eigenfrequencies has been introduced in Karageorghis (2001), and applied for simple shapes. Later, in Chen, Chang, Chen, and Chen (2005) it was studied the application of the MFS for the eigencalculation of multiply connected domains. It was found the appearance of spurious solutions and to filter them out they applied the singular value decomposition (SVD) and the Burton and Miller method. In Karageorghis (2001) it is presented a comparison with the boundary element method used in De Mey (1976), and the results obtained for simple shapes (circles, squares), show a better performance for the MFS. The application of other meshless methods to the determination of eigenfunctions and eigenmodes has also been subject to recent research, mainly using radial basis functions (e.g. Chen, Chang, Chen, and Lin (2002), Chen, Chang, Chen, and Chen (2002)) or the method of particular solutions (cf. Betcke and Trefethen (2005)).

Here we consider the application of the MFS to general simply connected shapes. In this case the choice of the source points in the MFS becames more important to retrieve with accuracy the eigenfrequencies. We are able to obtain good results introducing an algorithm that associates the source points to the shape. Having determined an approximation of the eigenfrequency, we apply a new algorithm based on the MFS to obtain the associated eigenmodes.

[1] CEMAT, Department of Mathematics, Instituto Superior Técnico, Av. Rovisco Pais 1, 1049-001 Lisboa, Portugal. (calves@math.ist.utl.pt; pant@math.ist.utl.pt)

2 Helmholtz equation

Let $\Omega \subset \mathbb{R}^2$ be a bounded simply connected domain with regular boundary $\partial\Omega$. For simplicity we will consider the 2D - Dirichlet eigenvalue problem for the Laplace operator. This is equivalent to obtain the resonance frequencies κ that satisfy the Helmholtz equation

$$\begin{cases} \Delta u + \kappa^2 u = 0 & \text{in } \Omega, \\ u = 0 & \text{on } \partial\Omega, \end{cases} \tag{1}$$

for a non null function u. As an application, this corresponds to recovering the resonance frequencies $\kappa > 0$ associated with a particular shape of a drum Ω.

A fundamental solution Φ_ω of the Helmholtz equation satisfies $(\Delta + \omega^2)\Phi_\omega = -\delta$, where δ is the Dirac delta distribution. In the 2D case, we take

$$\Phi_\omega(x) = \frac{i}{4} H_0^{(1)}(\omega|x|) \tag{2}$$

where $H_0^{(1)}$ is the first Hänkel function.

A density result in Alves and Chen (2005) states that if ω is not an eigenfrequency for the domain Ω then

$$L^2(\partial\Omega) = \overline{\text{span}\left\{\Phi_\omega(x-y)|_{x\in\partial\Omega} : y \in \hat{\Gamma}\right\}}, \tag{3}$$

where $\hat{\Gamma}$ is an admissible source set as defined in Alves and Chen (2005), for instance, the boundary of a bounded open set $\hat{\Omega} \supset \overline{\Omega}$, considering $\hat{\Gamma}$ surrounding $\partial\Omega$.

Definition 1 *The MFS approximations in the discrete set* $\hat{\Gamma}_m = \{y_1, ..., y_m\} \subseteq \hat{\Gamma}$ *are elements of the linear space* $V_m = span\{\Phi_\omega(\bullet - y_1), ..., \Phi_\omega(\bullet - y_m)\}|_{\partial\Omega}$

The result (3) allows to justify the approximation of a $L^2(\partial\Omega)$ function, with functions in V_m using a sequence of functions (u_m) with

$$u_m(x) = \sum_{j=1}^{m} \alpha_{m,j} \Phi_\omega(x - y_{m,j}), \quad (y_{m,j} \in \hat{\Gamma}) \tag{4}$$

that converges to $u|_\Gamma$ in $L^2(\partial\Omega)$. This is a partial justification to the convergence of the Method of Fundamental Solution (MFS) based on density results. It is similar to the approach in Bogomolny (1985), but it avoids the use of boundary layer potentials. As pointed out in Alves and Chen (2005), the convergence of the MFS, in a general case, is not completely related to the discretization of a single layer potential, although there is a straightforward relation. A single layer potential defined on $\hat{\Gamma}$ is an analytic function in Ω, and therefore such an approach would only be appropriate for analytic functions. Since $u|_\Gamma \equiv 0$ is an analytic function, here it makes sense to consider the approach of the MFS as being related to the discretization of the single layer potential, for $x \notin \hat{\Gamma}$,

$$\begin{aligned} \mathcal{S}_\omega\varphi(x) &= \int_{\hat{\Gamma}} \Phi_\omega(x-y)\varphi(y)\, ds_y \approx u_m(x) \\ &= \sum_{j=1}^{m} \alpha_{m,j} \Phi_\omega(x - y_{m,j}). \end{aligned} \tag{5}$$

Theorem 1 *If* ω *is not an eigenfrequency of the interior Dirichlet problem then* $dim(Ker(\mathcal{S}_\omega)) = 0$.

Proof. If ω is not an eigenfrequency then $\mathcal{S}_\omega\varphi = 0$ on $\partial\Omega$ implies $\mathcal{S}_\omega\varphi = 0$ in Ω, by the well posedness of the interior Dirichlet problem. Using the analyticity of $\mathcal{S}_\omega\varphi$, this implies $\mathcal{S}_\omega\varphi = 0$ in $\hat{\Omega}$ and the continuity of the traces implies $(\mathcal{S}_\omega\varphi)^+ = (\mathcal{S}_\omega\varphi)^- = 0$ on $\hat{\Gamma}$. Therefore, by the well posedness of the exterior Dirichlet problem, with the Sommerfeld radiation condition (verified by $\mathcal{S}_\omega\varphi$), this implies $\mathcal{S}_\omega\varphi = 0$ in $\mathbb{R}^2$. In conclusion, $\mathcal{S}_\omega\varphi = 0$ on $\partial\Omega$ implies $\varphi = 0$, and therefore $\dim(Ker(\mathcal{S}_\omega)) = 0$.

$\diamondsuit$

Thus, using this result, we search for ω such that $\dim(Ker(\mathcal{S}_\omega)) \neq 0$. These ω will be the eigenfrequencies for the Laplace-Dirichlet operator in Ω.

Note that instead of using a single layer representation in (5) it is also possible to use double layer representation (eg. Chen, Chang, Chen, and Chen (2005)).

3 Numerical Method using the MFS

3.1 Determination of the eigenfrequencies with Dirichlet boundary condition

From the previous considerations we present a procedure to find the eigenfrequencies by checking the frequencies ω for which $\dim(Ker(\mathcal{S}_\omega)) \neq 0$. Defining m collocation points $x_i \in \partial\Omega$ and m source points $y_{m,j} \in \hat{\Gamma}$,we obtain the system

$$\sum_{j=1}^{m} \alpha_{m,j} \Phi_\omega(x_i - y_{m,j}) = 0, \quad (x_i \in \partial\Omega). \tag{6}$$

Therefore a straighforward procedure is to find the values ω for which the $m \times m$ matrix

$$A(\omega) = [\Phi_\omega(x_i - y_j)]_{m\times m} \tag{7}$$

has a null determinant. However, an arbitrary choice of source points may lead to worst results than the expected with the MFS applied to simple shapes as in Karageorghis (2001). We will choose uniformly on the boundary $\partial\Omega$ the points $x_1,...,x_m$ (cf. Alves and Valtchev (2005)) and $y_1,...,y_m \in \hat{\Gamma}$ in a particular way. Given an integer m, the collocation points are obtained (cf. Alves and Valtchev (2005)) recursively such that $|x_{i+1} - x_i| = |\partial\Omega|/m$, and we take m point sources

$$y_i = x_i + \beta\frac{\tilde{\mathbf{n}}_i}{|\tilde{\mathbf{n}}_i|}$$

where $\tilde{\mathbf{n}}_i$ is approximately normal to the boundary $\partial\Omega$ on x_i. The vector $\tilde{\mathbf{n}}_i$ will be given by

$$\tilde{\mathbf{n}}_i = \frac{(\Delta x_i)^\perp + (\Delta x_{i+1})^\perp}{2}$$

where $\Delta x_i = x_i - x_{i-1}$ and $v^\perp = (v_1, v_2)^\perp = (-v_2, v_1)$. The parameter β is a constant value choosen such that:

(i) the source points remain outside Ω (in convex shapes it is sufficient to consider $\beta > 0$).

(ii) by experimental criteria obtained with simple shapes $m\beta/|\Omega|$ can not be too large.

The components of the matrix $A(\omega)$ are complex numbers, so the determinant is also a complex number. We consider the real function $g(\omega) = |Det[A(\omega)]|$. It is clear that the function g will be very small in any case, since the MFS is highly ill conditioned and the determinant is quite small.

Golden Ratio Search. To search for the point where the minimum is attained we use an algorithm based on the golden ratio search method. First we plot the graph of $\log(g(\omega))$ using a fewer number of points to choose an interval $]a,b[$ where there is only one eigenfrequency. Then we choose an error tolerance ε and we define $r_1 = \frac{\sqrt{5}-1}{2}$, $r_2 = r_1^2$ and the sets

$$X^0 = \left\{a_0^0, a_1^0, a_2^0, a_3^0\right\}$$

and

$$G^0 = \left\{g_0^0, g_1^0, g_2^0, g_3^0\right\}$$

where $a_0^0 = a$, $a_1^0 = a + (b-a)r_2$, $a_2^0 = a + (b-a)r_1$, $a_3^0 = b$ and $g_i^0 = g\left(a_i^0\right)$. As the function g is supposed to have only one minimum in the interval $]a,b[$, we have

$$min\left\{g(a_0^0), g(a_3^0)\right\} > max\left\{g(a_1^0), g(a_2^0)\right\}$$

so $minG^0$ is attained at a_1^0 or a_2^0. Then for $k = 1,2,...$ while $|a_3^k - a_0^k| > \varepsilon$,

if $g_1^0 \le g_2^0$ then we define the sets

$$X^k = \left\{a_0^{k-1}, a_1^k = a_0^{k-1} + (a_3^{k-1} - a_0^{k-1})r_2, a_1^{k-1}, a_2^{k-1}\right\}$$

$$G^k = \left\{g_0^{k-1}, g_1^k, g_1^{k-1}, g_2^{k-1}\right\}$$

else if $g_1^0 > g_2^0$ we define the sets

$$X^k = \left\{a_1^{k-1}, a_2^{k-1}, a_2^k = a_0^{k-1} + (a_3^{k-1} - a_0^{k-1})r_1, a_3^{k-1}\right\}$$

$$G^k = \left\{g_1^{k-1}, g_2^{k-1}, g_2^k, g_3^{k-1}\right\}$$

In each new iteration we only need to evaluate the function once. This method showed itself to be quite accurate.

Repeating some calculations of Chen, Kuo, Chen, and Cheng (2000) or Chen, Chang, Chen, and Chen (2005) we can prove that for a circular domain with radius ρ, if we place $2N$ collocation points uniformly distributed on the boundary and $2N$ points on the boundary of a circular domain with radius $R > \rho$ then the eigenvalues of the stiffness matrix are such that

$$\lambda_m \overset{N\to\infty}{\to} 2NJ_m(\omega\rho)H_m^{(1)}(\omega R),$$
$$m = 0, \pm1, \pm2, ..., \pm(N-1), N$$

where J_m is the first kind of the m^{th} order Bessel function. So we have

$$g(\omega) \overset{N\to\infty}{\longrightarrow} 2N \prod_{m=-(N-1)}^{N} \left|J_m(\omega\rho)H_m^{(1)}(\omega R)\right|.$$

3.2 Determination of the eigenmodes with Dirichlet boundary condition

To obtain an eigenfunction associated with a certain resonance frequency κ we use a collocation method on $n+1$

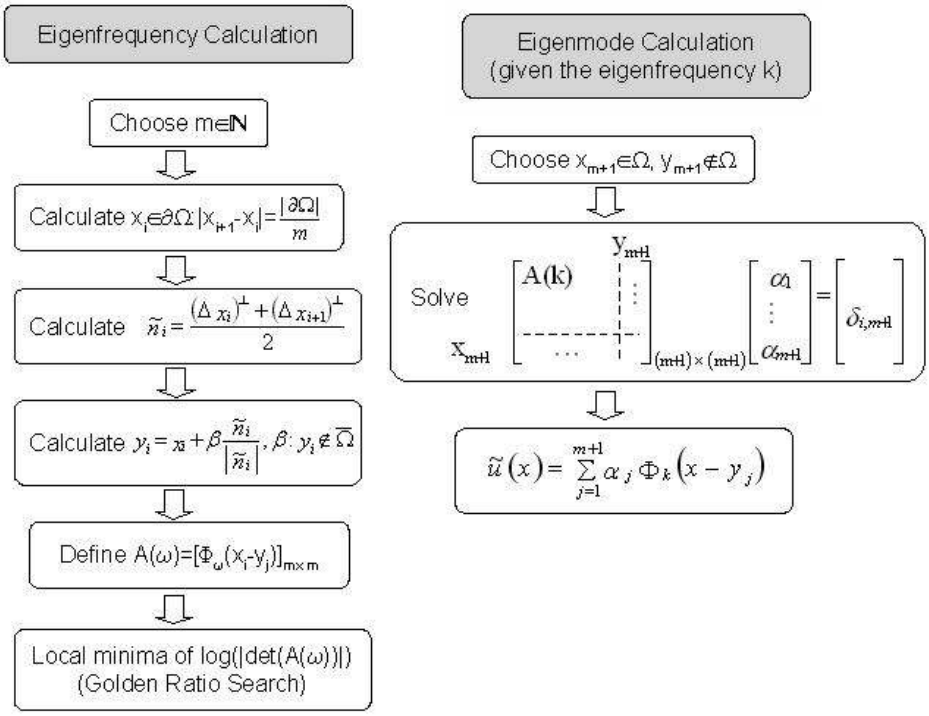

points, with $x_1, \cdots, x_n$ on $\partial\Omega$ and a point $x_{n+1} \in \Omega$. Then, the approximation of the eigenfunction is given by

$$\tilde{u}(x) = \sum_{j=1}^{n+1} \alpha_j \Phi_\kappa(x - y_j). \tag{8}$$

To exclude the solution $\tilde{u}(x) \equiv 0$, the coefficients α_j are determinated by the solution of the system

$$\begin{cases} \tilde{u}(x_i) = 0, & i = 1, \ldots, n \\ \tilde{u}(x_{n+1}) = 1 \end{cases} \tag{9}$$

When we take $n = m$ this resumes to add one line and one column to the matrix $A(\omega)$ defined in (19).

This procedure may fail if the selected point x_{n+1} is on the nodal line (cf. Chen, Chen, and Chyuan (1999), Chen, Huang, and Chen (1999)). Depending on the multiplicity of the eigenvalue, we will add one or more collocation points to make the linear system well determined. A simplified version of the method is presented in the flowchart. The eigenmode calculation may be better using a different choice of collocation points x_i and a different choice of source points y_j (by changing β).

3.3 Error bounds

An error bound can be derived using the following result (cf. Moler and Payne (1968)).

Theorem 2 *Let $\tilde{\kappa}$ and $\tilde{u} \in C^2(\Omega) \cap C(\overline{\Omega})$ be an approximate eigenfrequency and eigenfunction which satisfy the following problem:*

$$\begin{cases} \Delta\tilde{u} + \tilde{\kappa}^2\tilde{u} = 0 & \text{in } \Omega \\ \tilde{u} = \varepsilon(x) & \text{on } \partial\Omega \end{cases} \tag{10}$$

Then there exists an eigenfrequency κ_p such that

$$\frac{|\kappa_p - \tilde{\kappa}|}{|\kappa_p|} \leq \theta \tag{11}$$

where

$$\theta = \frac{\sqrt{|\Omega|}\,\|\varepsilon\|_{L^\infty(\partial\Omega)}}{\|\tilde{u}\|_{L^2(\Omega)}} \tag{12}$$

where $|\Omega|$ is the area of the domain Ω. If in addition, $\|\tilde{u}\|_{L_2(\Omega)} = 1$ and u is the normalized orthogonal projec-

tion of $\tilde{u}$ onto the eigenspace of κ_p, then

$$\|u-\tilde{u}\|_{L^2(\Omega)} \leq \frac{\theta}{\rho_p}\left(1+\frac{\theta^2}{\rho_p^2}\right)^{\frac{1}{2}} \tag{13}$$

where

$$\rho_p := min_{\kappa_n \neq \kappa_p} \frac{\left|\kappa_n^2-\tilde{\kappa}^2\right|}{\kappa_n^2} \tag{14}$$

Proof. It follows immediately from a result due to Moler and Payne (cf. Moler and Payne (1968)) since

$$\begin{aligned}\frac{|\kappa_p-\tilde{\kappa}|}{|\kappa_p|} &\leq \frac{|\kappa_p-\tilde{\kappa}|}{|\kappa_p|}\frac{|\kappa_p+\tilde{\kappa}|}{|\kappa_p|} \\ &= \frac{\left|\kappa_p^2-\tilde{\kappa}^2\right|}{\left|\kappa_p^2\right|} = \frac{\left|\lambda_p-\tilde{\lambda}\right|}{|\lambda_p|} \leq \theta\end{aligned} \tag{15}$$

♢

Note also that using the inequality (11) we can easily obtain

$$|\kappa_p-\tilde{\kappa_p}| \leq \left(\frac{\theta}{1-\theta}\right)\tilde{\kappa_p}. \tag{16}$$

3.4 *Determination of the eigenfrequencies with Neumann boundary condition*

Defining m collocation points $x_i \in \partial\Omega$ and m source points $y_{m,j} \in \hat{\Gamma}$, as in the Dirichlet case we obtain the system

$$\sum_{j=1}^{m} \alpha_{m,j}\, \partial_n \Phi_\omega(x_i-y_{m,j}) = 0, \quad (x_1,\ldots,x_m \in \partial\Omega) \tag{17}$$

where ∂_n is the outnormal derivative. Defining the function

$$\hat{\Phi}_\omega(x) = \frac{i}{4}H_1^{(1)}(\omega|x|) \tag{18}$$

we obtain the system

$$\begin{aligned}\partial_n(\tilde{u}(x_i)) &= \sum_{j=1}^{m} \alpha_{m,j}\omega\, \tilde{n}.\frac{x_i-y_j}{|x_i-y_j|}\hat{\Phi}_\omega(\omega|x_i-y_j|) \\ &= 0, \quad i=1,\ldots,m\end{aligned}$$

where $\tilde{n}$ is an approximation for unitary vector which is normal to the boundary $\partial\Omega$ on the point x_i. Therefore the procedure is to search the values ω for which the $m\times m$ matrix

$$A(\omega) = \left[\tilde{n}.\frac{x_i-y_j}{|x_i-y_j|}\hat{\Phi}_\omega(\omega|x_i-y_j|)\right]_{m\times m} \tag{19}$$

has a null determinant.

3.5 *Determination of the eigenmodes with Neumann boundary condition*

As in the Dirichlet case, for an eigenfrequency κ we use a collocation method on $n+1$ points, with $x_1,\cdots,x_n$ on $\partial\Omega$ and a point $x_{n+1} \in \Omega$ (again, as in the Dirichlet case, x_{n+1} should not be chosen on the nodal line). The approximation of the eigenfunction is given by

$$\tilde{u}(x) = \sum_{j=1}^{n+1} \alpha_j \Phi_\kappa(x-y_j). \tag{20}$$

The coefficients α_j are determinated by the solution of the system

$$\begin{cases} \partial_n(\tilde{u}(x_i)) = 0, & i=1,\ldots,n \\ \tilde{u}(x_{n+1}) = 1. \end{cases} \tag{21}$$

4 Numerical Results

4.1 *Dirichlet boundary condition.*

4.1.1 *Calculation of the eigenfrequencies.*

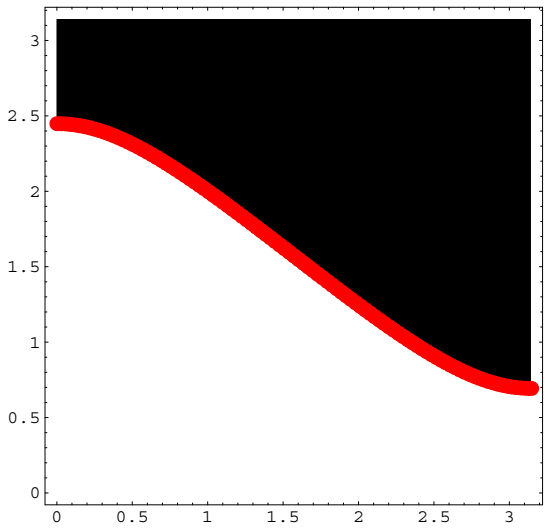

Figure 1 : nodal line of the eigenfunction associated with the 2^{nd} eigenfrequency of the square.

Table 1 : absolute errors for the former three modes of the disk

m	abs. error (κ_1)		m	abs. error (κ_2)		m	abs. error (κ_3)
60	8.23746×10^{-11}		60	9.30012×10^{-12}		60	9.35225×10^{-11}

Table 2 : absolute errors for the former three modes of the square

m	abs. error (κ_1)		m	abs. error (κ_2)		m	abs. error (κ_3)
60	1.46642×10^{-9}		60	1.44218×10^{-9}		60	3.17219×10^{-9}

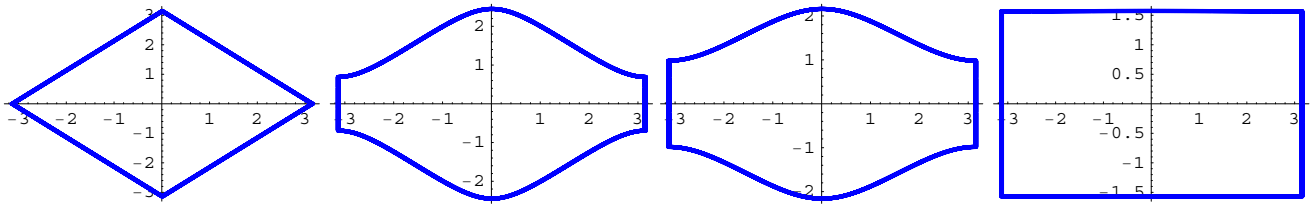

Figure 2 : domains obtained for $c = 1$, $c = 1.3$, $c = 1.8$ and $c = 600$ (resp.).

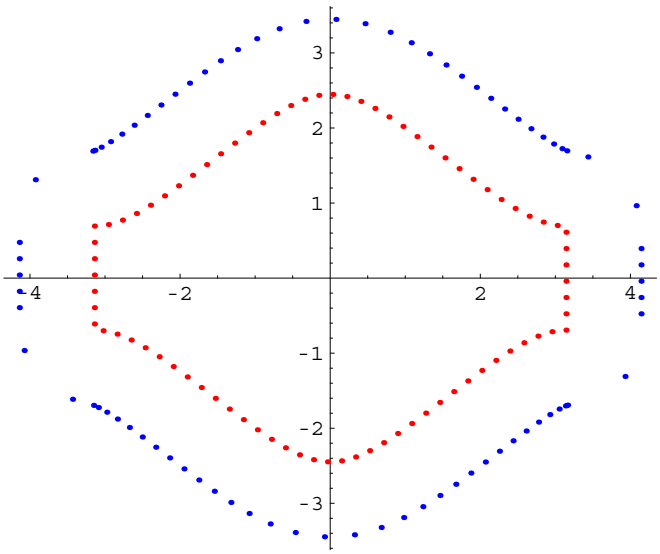

Figure 3 : collocation points and point sources with $m = 80$ and $\beta = 1$.

Since the values of the eigenfrequencies for the unit disk are well known, given by a Bessel function, we will first test the results of this method for the former three modes considering $\beta = 0.4$ (Tab. 1)

and for the unit square we obtain the following results for the former three modes considering $\beta = 0.4$ (Tab. 2).

Now we will apply the numerical method to a domain for which the 5^{th} resonance frequency is known. It's well known that the functions $v(x,y) = c\sin(x)\sin(2y) + \sin(2x)\sin(y)$ are the eigenfunctions associated to the value $\sqrt{5}$, the second eigenfrequency of the square $[0,\pi] \times [0,\pi]$. We can write the functions v as $v(x,y) = 2\sin(x)\sin(y)[c\cos(y) + \cos(x)]$. So, for $c \in [1,\infty[$ the respective nodal lines are given by $y = arcos(\frac{-1}{c}\cos(x))$, $x \in [0,\pi]$ (Fig. 1).

Then, the value $\kappa_5 = \sqrt{5}$ is the 5^{th} eigenfrequency of each of the the domains presented in Fig. 2. The domains obtained for the different values $c \in [0,\infty[$ have the same area and the same 5^{th} resonance frequency. In the cases $c = 1$ and $c \to \infty$ we obtain (resp.) the square with length side π and a rectangle with length sides 2π and π.

For $c = 1.3$ and $\beta = 1$ we obtain the points plotted in Fig. 3 and the values of the absolute errors in Tab. 3.

We can use the same procedure to find the nodal line of another eigenfunction of the square. We know that the functions $v(x,y) = c\sin(x)\sin(3y) + \sin(3x)\sin(y)$ are the eigenfunctions associated with the eigenfrequency $\sqrt{10}$. We can rewrite the function v as

$$v(x,y) = \sin(x)\sin(y)\left(3 - 4\sin^2(x) + c(3 - 4\sin^2 y)\right).$$

So the nodal line is given by the implicit equation

$$\sin^2(y) = \frac{3 + \frac{3-4\sin^2(x)}{c}}{4}$$

Chosing $c = 3$ we obtain the domain plotted in Fig. 4. For this domain the first eigenfrequency is exactly $\sqrt{10}$.

Table 3 : absolute errors with $\beta = 1$

m	abs. error (κ_5)	m	abs. error (κ_5)	m	abs. error (κ_5)
20	2.10352×10^{-4}	30	1.46198×10^{-5}	40	1.2331×10^{-6}
50	3.06129×10^{-7}	60	2.52128×10^{-8}	70	5.05447×10^{-9}
80	3.19481×10^{-9}	90	6.19889×10^{-10}	100	1.87289×10^{-10}

Table 4 : absolute errors with the proposed choice of point-sources

m	abs. error (κ_1)	m	abs. error (κ_1)	m	abs. error (κ_1)
60	3.90501×10^{-11}	70	3.12239×10^{-12}	80	5.81756×10^{-14}

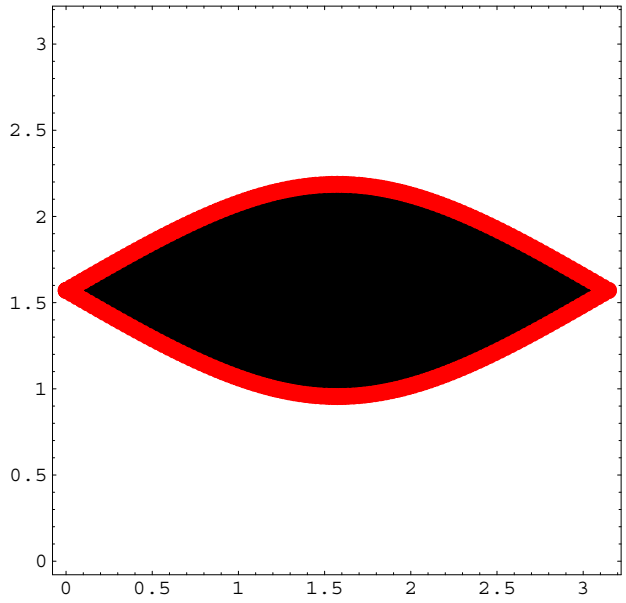

Figure 4 : nodal line of the eigenfunction associated with the eigenfrequency $\sqrt{10}$ (for $c = 3$).

We will now consider three cases of different choices for the point-sources. In the first case we consider as artificial boundary the "expansion" of the boundary of the domain; in the second case we consider the boundary of a circular domain and in the last case we consider our choice with $\beta = 1$ (Fig. 5).

In Fig. 6 we present the plot of $\log(g(\omega))$ with the points plotted in Fig. 5. We note that in Fig. 6 the first two plots present rounding errors generated by the ill conditioned matrix. With the proposed choice of points the ill conditioning decreases and the rounding errors are much smaller (third plot).

Table 5 : absolute errors of the second and third eigenfrequencies

m	abs. error (κ_2)	abs. error (κ_3)
60	1.15174×10^{-10}	1.25×10^{-10}
70	4.16147×10^{-11}	6.83542×10^{-12}
80	3.336×10^{-12}	5.03242×10^{-12}

With the proposed choice of point-sources we obtain the absolute errors in Tab. 4.

The method revealed to be very accurate for the search of eigenfrequencies even in the case of eigenfrequencies near to each other. It's well known that the second eigenfrequency of the square has multiplicity two. We will consider a rectangular domain with length sides 1 and $1 + 10^{-8}$. Since we have an explicit formula for all the eingenfrequencies of a rectangular domain (eg. Courant and Hilbert (1953)), it is easy to prove that $\kappa_3 - \kappa_2 \approx 4.215 \times 10^{-8}$ and we obtain the results in Tab. 5 for the absolute error of the second and third eigenfrequencies with $\beta = 0.5$.

In this case, if we consider less than 60 points, the method is not able to recover the two eigenfrequencies as we can see in Fig. 7. We present the plot of $\log(g(\omega))$ for $\omega \in [7.02481465, 7.02481474]$. In each case, we represent with larger (red) points the two exact eigenfrequencies.

4.1.2 Calculation of the eigenmodes.

In Fig. 8 we present the plot of the points considered to obtain the eigenfunctions of the domain Ω_1 with bound-

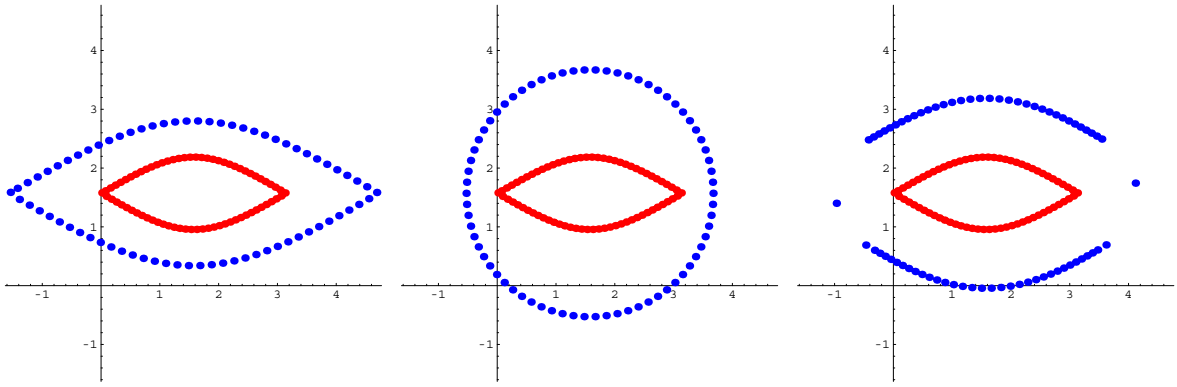

Figure 5 : collocation points and three different choices for the point-sources with $m = 70$.

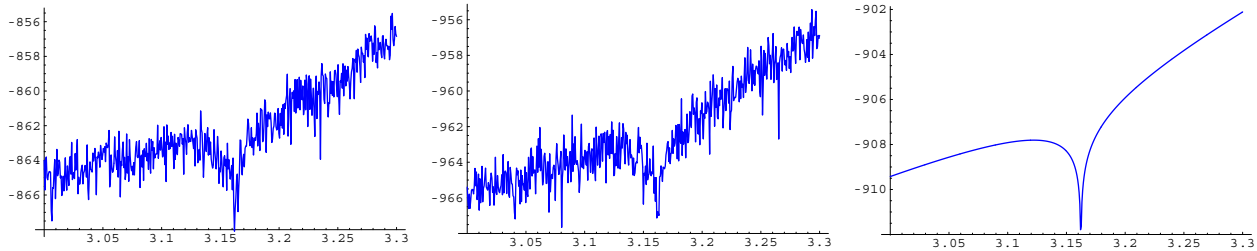

Figure 6 : plot of the function $\log(g(\omega))$ with $m = 70$ for three choices of points.

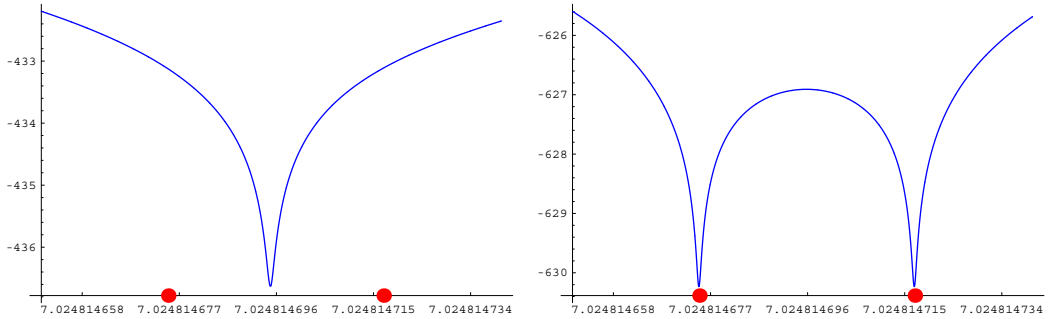

Figure 7 : plot of the function $\log(g(\omega))$ with $m = 50$ and $m = 60$.

ary given by the parametrization

$$t \mapsto \left(\cos(t), \sin(t) + \frac{5\sin(t)\cos(2t)}{9}\right)$$

In Fig. 9 we show the plots of eigenfunctions associated with the 21^{th} and 22^{th} eigenfrequencies for the domain Ω_1. In top of each picture it is written the associated eigenfrequency. The resonance frequency was obtained with $\beta = 0.25$ and $m = 120$; the eigenfunction with $\beta = 0.25$ and $n = 150$.

In Fig. 10 we present the respective nodal domains (ie. the domains for where the real eigenfunction keeps the same sign)

In Fig. 11 and Fig. 12 we present the same plots (associated with the 20^{th} and 26^{th} eigenfrequencies) now con-

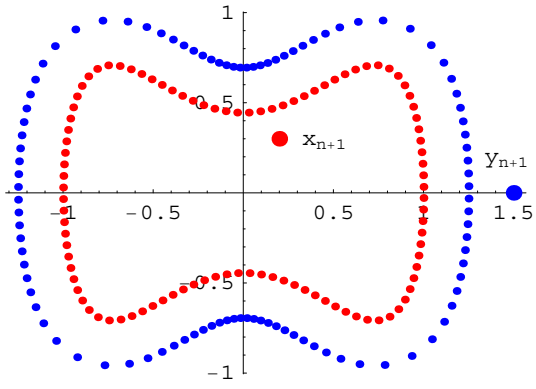

Figure 8 : plot of the points considered to obtain the eigenfunctions of the domain Ω_1.

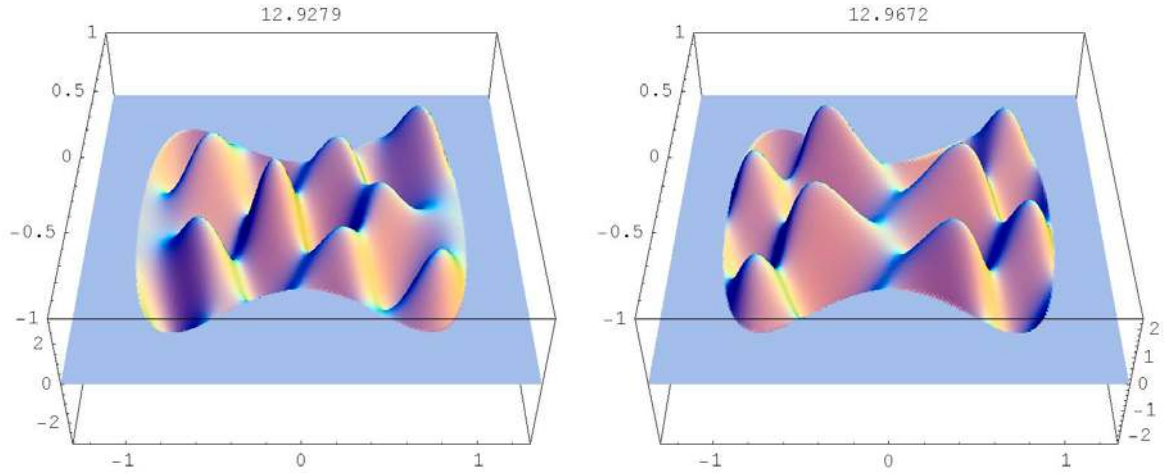

Figure 9 : eigenfunctions associated with the 21^{th} and 22^{th} eigenfrequencies of the domain Ω_1.

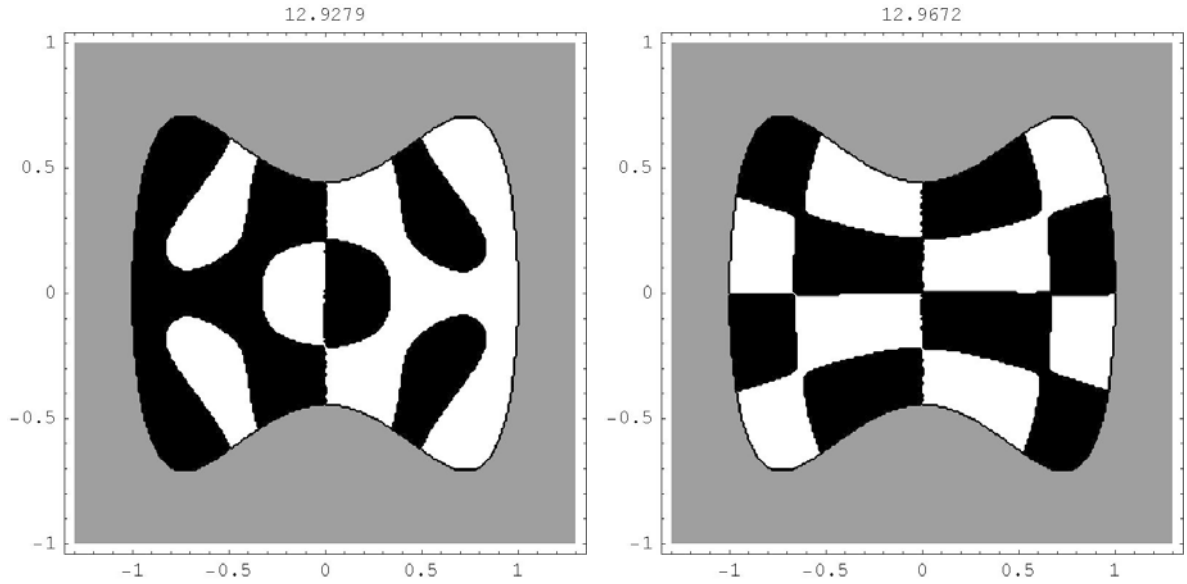

Figure 10 : nodal domains of the eigenfunctions associated with the 21^{th} and 22^{th} eigenfrequencies of the domain Ω_1.

sidering a domain Ω_2 with boundary given by

$$t \mapsto \left(16.8\cos(t), 8\left(\sin(t)+\frac{5}{9}\sin(t)\cos(4t)\right)+3\cos(2t)\right)$$

The resonance eigenfrequency was obtained with $\beta = 3$ and $m = 170$; the eigenfunction was obtained with $\beta = 0.3$ and $n = 180$.

Using the MFS we obtain the eigenfunction defined over all the points of the domain. This allows us to answer some questions: we may be interested to count the nodal domains associated with a certain eigenfrequency. For example, in the second plot of Fig. 10, we must study the nodal lines. In Fig. 13 we present the sign of the eigenfunction on a linear curve that connects the points $(0.5, 0.15)$ and $(0.75, 0.47)$. As we can view in the second plot of Fig. 13 the eigenfunction doesn't change of sign on this curve (the minimum on this curve ≈ 0.417).

4.2 Error Bounds: Dirichlet boundary conditions

In this section we will obtain bounds for the error of the numerical values obtained for the domain Ω_1.

4.2.1 Bounds for the error of the eigenfrequency.

In Fig. 14 we plot the values of $|\varepsilon(x)|$, on 1001 points on $\partial\Omega_1$ for the eigenfunctions $\tilde{u_1}$ and $\tilde{u_2}$. We have $\|\varepsilon\|_{L^\infty(\partial\Omega_1)} \approx 9.469 \times 10^{-15}$ and 1.355×10^{-13} (resp.),

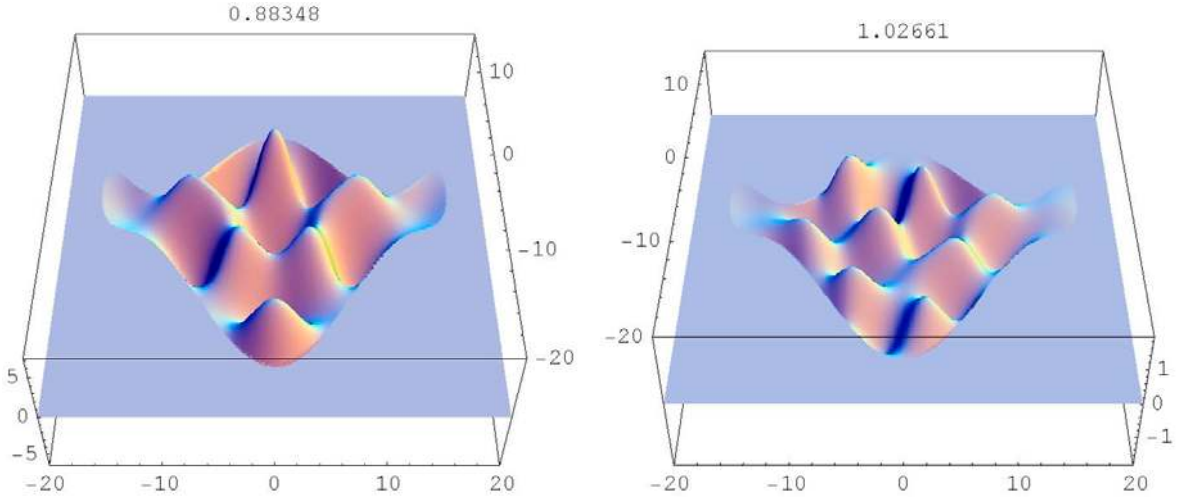

Figure 11 : eigenfunctions associated with the 20^{th} and 26^{th} eigenfrequencies of the domain Ω_2.

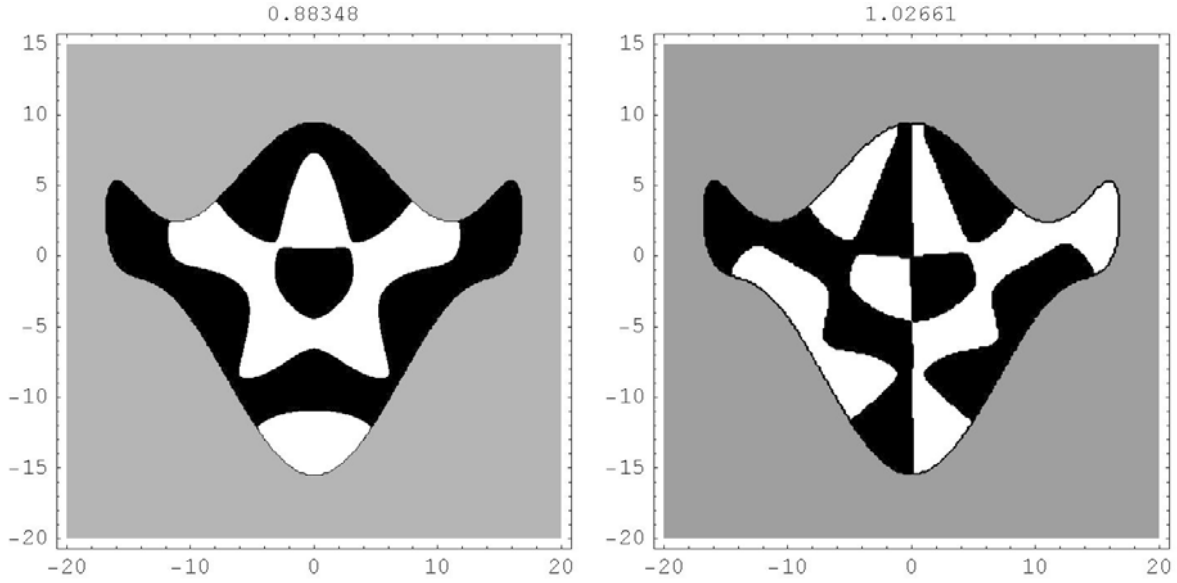

Figure 12 : nodal domains for the eigenfunctions associated with the 20^{th} and 26^{th} eigenfrequencies of the domain Ω_2.

$|\Omega_1| \approx 2.2689$ and we obtain that $\|\tilde{u_1}\|_{L^2(\Omega_1)} = 1.085$ and 0.902 (resp.). By (16) we obtain the bounds

$$|\kappa_1 - \tilde{\kappa}| \leq 1.577 \times 10^{-13}$$

and

$$|\kappa_2 - \tilde{\kappa}| \leq 3.949 \times 10^{-12}.$$

4.2.2 Bounds for the error of the eigenmodes.

We have $\rho_1 = |\lambda_1 - \lambda_2| = 5.453$ and as the third eigenvalue is (approx.) equal to 30.728, $\rho_2 = min\{|\lambda_1 - \lambda_2|, |\lambda_3 - \lambda_2|\} = min\{5.453, 13.267\} = 5.453$ and we obtain

$$\|u_1 - \tilde{u_1}\|_{L_2(\Omega_1)} \leq 2.898 \times 10^{-15}$$

and

$$\|u_2 - \tilde{u_2}\|_{L_2(\Omega_1)} \leq 4.147 \times 10^{-14}.$$

We obtain the following results:
with $m = 190$, $\tilde{\kappa_1} = 3.465228791746209$ and $\tilde{\kappa_2} = 4.178634826067797$. The results obtained with $m = 180$ differ from these to order 10^{-16}, so we expect that the errors are of this order.

4.3 The Stadium conjecture

Now we apply the numerical method to a well known problem. In Troesch (1973) it was formulated the conjecture that the stadium (the convex hull of two identical

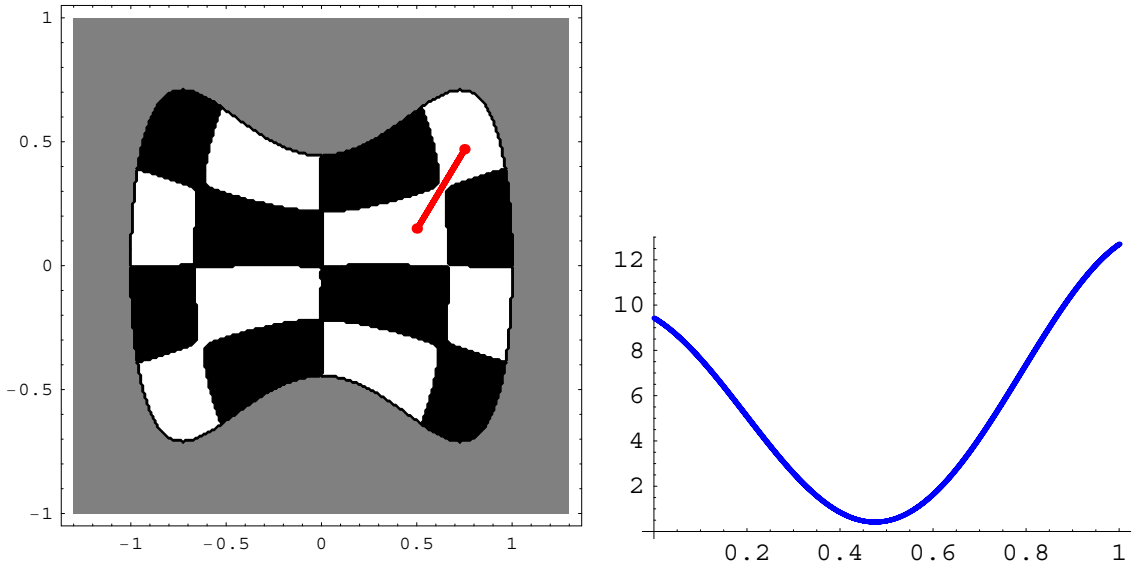

Figure 13 : nodal domains of the eigenfunction associated with the 22^{th} eigenfrequency of the domain Ω_1 and the sign of the eigenfunction on the curve presented.

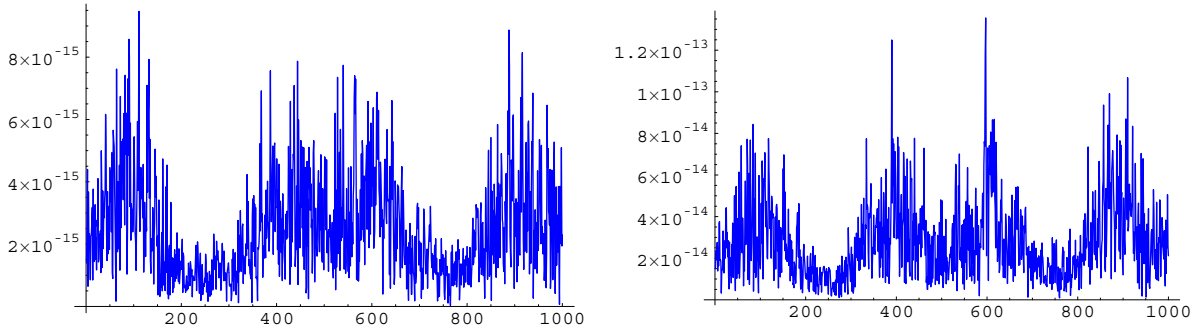

Figure 14 : values of $|\varepsilon(x)|$ on $\partial\Omega_1$ for the two eigenfunctions $\tilde{u_1}$ e $\tilde{u_2}$ (resp.).

tangent balls) was the open set of the plane which minimizes the second Dirichlet eigenvalue. This conjecture was refuted in Henrot and Oudet (2001). In Oudet (2004) it was proposed an optimization algorithm which allowed to obtain a domain with a second eigenvalue which is smaller than the value of the stadium. However, it wasn't presented an analytic expression for the domain. We are able to specify some domains which have the second eigenvalue smaller than the stadium. Consider the domain ploted in Fig. 15 which is the union of a rectangle and two half of ellipses. The stadium is the particular case of $L_1 = L_2 = 2R$. We will consider domains with unit area, so we have $L_1 = \frac{2-\pi L_2 R}{2L_2}$. Numerically we obtain that the domain whose second eigenvalue is smallest satisfies $L_2 \approx 0.7404695918$ and $R = 0.343193$. We call this domain Ω_4 and S to the stadium, both domains with

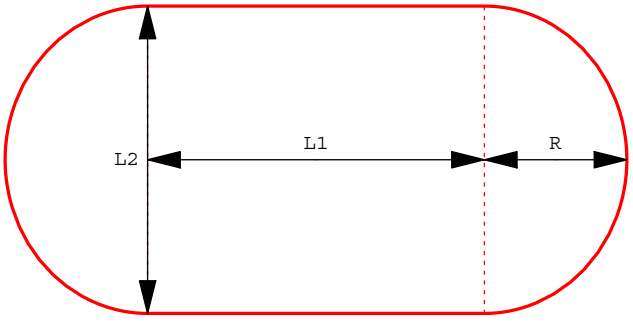

Figure 15 : plot of the proposed domain.

unit area. We obtain the following values

$$\lambda_2(\Omega_4) \approx 37.9875443; \lambda_2(S) \approx 38.0021483$$

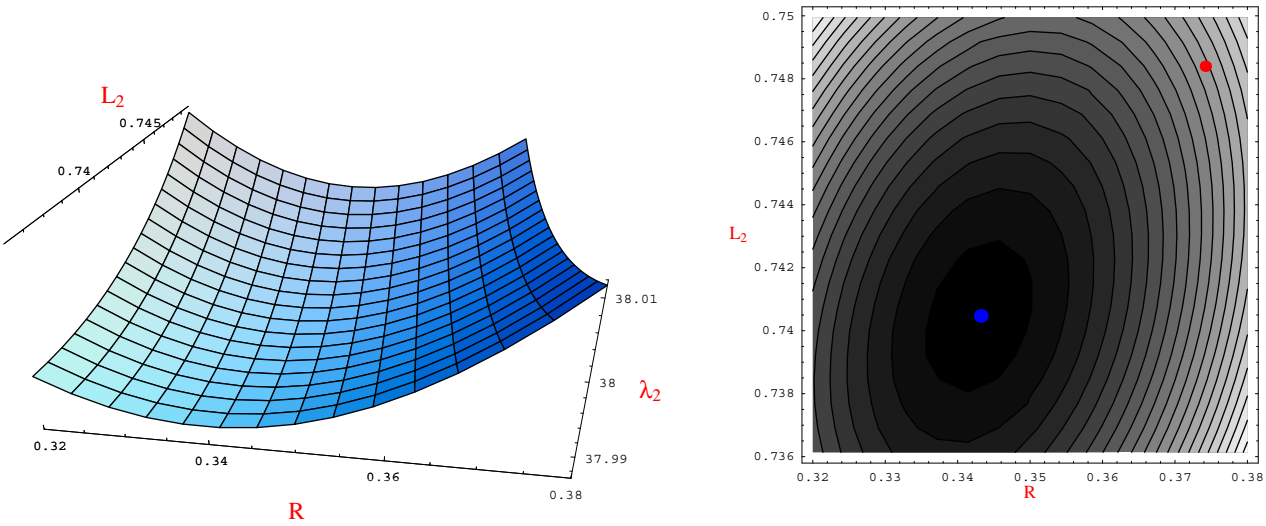

Figure 16 : plot and contour plot of the second eigenvalue as function of r and L_2.

In Fig. 16 we present the plot and the contour plot of the second Dirichlet eigenvalue as function of R and L_2 for some of the proposed domains. In the second plot we mark the stadium and the domain Ω_4. Using Theorem 2 we can obtain the bounds $\lambda_2(\Omega_4) \leq 37.98771 < 38.00194 \leq \lambda_2(S)$ which proves that $\lambda_2(\Omega_4) < \lambda_2(S)$.

4.4 Neumann boundary conditions

4.4.1 Calculation of the eigenfrequencies.

Now we will first test the results of this method for the former three modes of the unit disk considering $\beta = 2$ (Tab. 6). and for the unit square with $\beta = 2$ (Tab. 7).

4.4.2 Calculation of the eigenmodes.

Now we apply the method for domain Ω_3 with boundary given by the parametrization

$$t \mapsto \left(\cos(t), \sin(t) + \frac{\sin(2t)}{3}\right)$$

In Fig. 17 we show the plots of eigenfunctions associated with the 21^{th} and 26^{th} eigenfrequencies of the domain Ω_3. The resonance frequency and the eigenfunction were obtained with $\beta = 0.4$ and $m = 100$.

In Fig. 18 we present the respective nodal domains.

5 Conclusion

In this brief account we presented the MFS method with an algorithm for the choice of source points that has already been tested to the determination of eigenfrequencies and eigenmodes for hundreds of non trivial domains (cf. Antunes and Freitas (2005)). We have presented some numerical results with a Fortran code running on a standard Laptop. The numerical calculations, made with double precision imply some limitations to the system dimension (we only considered up to 200×200 matrices). With the proposed choice of collocation and source points, a small dimension system allows very small errors, almost at machine precision level. This is no longer possible with more complicated shapes. In this global method approach more collocation points will be needed to approximate the shape, the dimension of the matrices will be larger and ill-conditioned. To decrease the ill-conditioning the source points should be closer to the boundary, leading to worst results. Another possibility is to consider local methods (eg. Han and Atluri (2004), Han and Atluri (2003), Grannell and Atluri (1967)).

Acknowledgement: This work was partially supported by FCT-POCTI/FEDER, project POCTI-MAT/34735/00, POCTI-MAT/60863/2004, POCTI-ECM/58940/2004 and NATO-PST.CLG.980398. We would like to thank our colleague P. Freitas for fruitful discussions.

Table 6 : absolute errors for the former three modes of the unit disk

m	abs. error (κ_1)		m	abs. error (κ_2)		m	abs. error (κ_3)
20	1.59019×10^{-10}		20	8.66227×10^{-9}		20	2.48929×10^{-9}
30	1.11022×10^{-14}		30	8.26005×10^{-14}		30	2.30926×10^{-14}

Table 7 : absolute errors for the former three modes of the unit square

m	abs. error (κ_1)		m	abs. error (κ_2)		m	abs. error (κ_3)
20	1.29506×10^{-6}		20	5.40504×10^{-7}		20	3.56705×10^{-6}
32	2.5788×10^{-10}		32	9.7475×10^{-10}		32	1.32234×10^{-9}

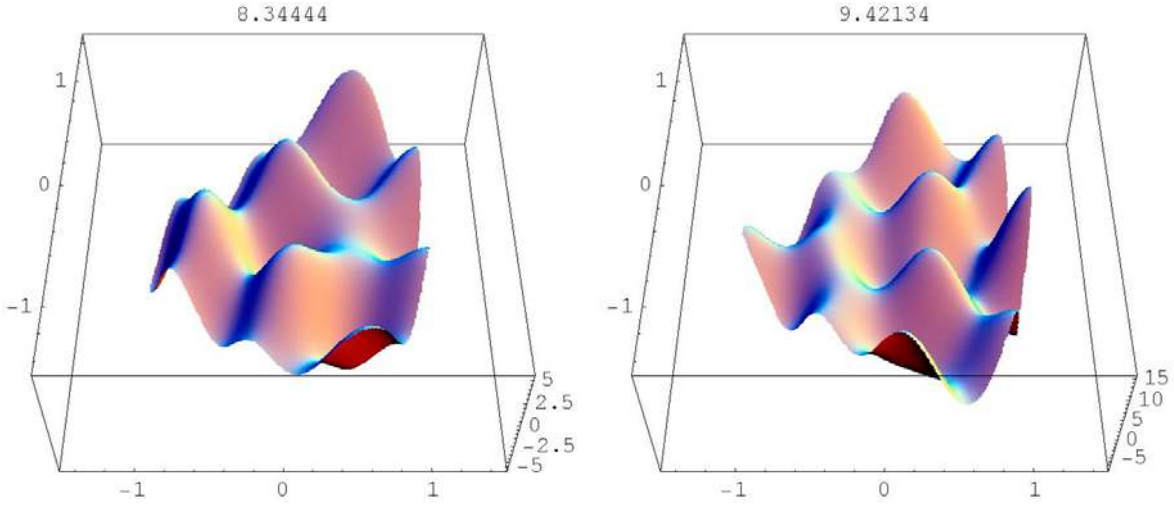

Figure 17 : eigenfunctions associated with the 21^{th} and 26^{th} eigenfrequencies of the domain Ω_3.

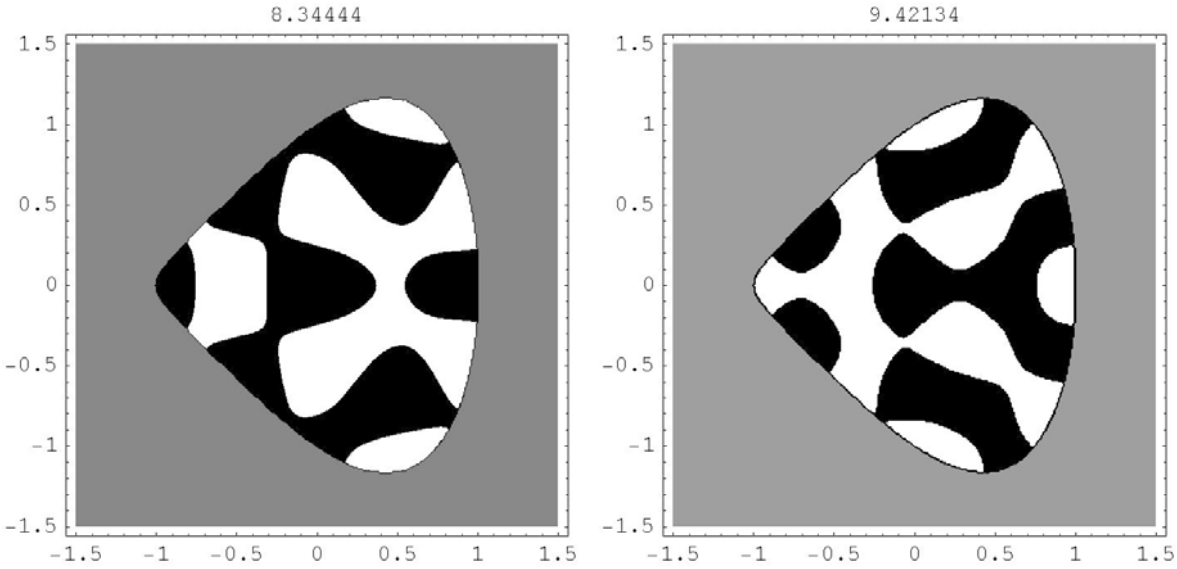

Figure 18 : nodal domains of eigenfunctions associated with the 21^{th} and 26^{th} eigenfrequencies of the domain Ω_3.

References

Alves, C. J. S.; Chen, C. S. (2005): A new method of fundamental solutions applied to nonhomogeneous elliptic problems. *Adv. Comp. Math.*, vol. 23, pp. 125–142.

Alves, C. J. S.; Valtchev, S. S. (2005): Numerical comparison of two meshfree methods for acoustic wave scattering. *Engineering Analysis with Boundary Elements*, vol. 29, pp. 371–382.

Antunes, P. R. S.; Freitas, P. (2005): New bounds for the principal Dirichlet eigenvalue of planar regions. *accepted*.

Arantes e Oliveira, E. R. (1968): Plane stress analysis by a general integral method. *Proc. ASCE Eng. Mech. Div.*, vol. 94, pp. 79–101.

Atluri, S. N. (2004): *The Meshless Method (MLPG) for domain & boundary discretizations*. Tech. Science Press, Forsyth.

Betcke, T.; Trefethen, L. N. (2005): Reviving the Method of Particular Solutions. *to appear in SIAM Review*.

Bogomolny, A. (1985): Fundamental Solutions Method for Elliptic Boundary Value Problems. *SIAM J. Numer. Anal.*, vol. 22, no. 4, pp. 644–669.

Chen, J. T.; Chang, M. H.; Chen, K. H.; Chen, I. L. (2002): Boundary collocation method for acoustic eigenalysis of three-dimensional cavities using radial basis function. *Computational Mechanics*, vol. 29, pp. 392–408.

Chen, J. T.; Chang, M. H.; Chen, K. H.; Chen, I. L. (2005): Eigensolutions of multiply connected membranes using the method of fundamental solutions. *Engineering Analysis with Boundary Elements*, vol. 29, no. 2, pp. 166–174.

Chen, J. T.; Chang, M. H.; Chen, K. H.; Lin, S. R. (2002): Boundary collocation method with meshless concept for acoustic eigenanalysis of two-dimensional cavities using radial basis function. *Journal of Sound and Vibration*, vol. 257, no. 4, pp. 667–711.

Chen, J. T.; Chen, K. H.; Chyuan, S. W. (1999): Numerical experiments for acoustic modes of a square cavity using the dual BEM. *Applied Acoustics*, vol. 57, no. 4, pp. 293–325.

Chen, J. T.; Huang, C. X.; Chen, K. H. (1999): Determination of spurious eigenvalues and multiplicities of the true eigenvalues using the real-part dual BEM. *Computational Mechanics*, vol. 24, no. 1, pp. 41–51.

Chen, J. T.; Kuo, S. R.; Chen, K. H.; Cheng, Y. C. (2000): Comments on "Vibration analysis of arbitrary shaped membranes using nondimensional dynamic influence function". *Journal of Sound and Vibration*, vol. 235, no. 1, pp. 156–171.

Courant, R.; Hilbert, D. (1953): *Methods of Mathematical Physics, vol. 1*. Interscience, New York.

Cox, S. J.; Uhlig, P. X. (2003): Where best to hold a drum fast. *SIAM Review*, vol. 45, no. 1, pp. 75–92.

De Mey, G. (1976): Calculation of the Eigenvalues of the Helmholtz Equation by an Integral Equation. *Int. J. Num. Meth. Eng.*, vol. 10, pp. 59–66.

Golberg, M. A.; Chen, C. S. (1996): *Discrete Projection Methods for Integral Equations*. Computational Mechanics, Southampton.

Grannell, J. J.; Atluri, S. N. (1967): Boundary Methods (BEM) and conbination of BEM-FEM. *SIAM J. Numer. Anal.*, vol. 4, pp. 89–102.

Han, Z. D.; Atluri, S. N. (2003): Truly Meshless Local Petrov-Galerkin (MLPG) solutions of traction & displacement BIEs. *CMES: Computer Modeling in Engineering & Sciences*, vol. 4, no. 6, pp. 665–678.

Han, Z. D.; Atluri, S. N. (2004): A Meshless Local Petrov-Galerkin (MLPG) approach for 3-dimensional elasto-dynamics. *CMC: Computers, Materials & Continua*, vol. 1, no. 2, pp. 129–140.

Henrot, A.; Oudet, E. (2001): Le stade ne minimize pas λ_2 parmi les ouverts convexes du plan. *C. R. Acad. Sci. Paris Sr I Math*, vol. 332, pp. 417–422.

Karageorghis, A. (2001): The Method of Fundamental Solutions for the calculation of the Eigenvalues of the Helmholtz Equation. *Appl Math. Letters*, vol. 14, no. 7, pp. 837–842.

Kupradze, V. D.; Aleksidze, M. A. (1964): The method of functional equations for the approximate solution of certain boundary value problems. *U.S.S.R. Computational Mathematics and Mathematical Physics*, vol. 4, pp. 82–126.

Moler, C. B.; Payne, L. E. (1968): Bounds for Eigenvalues and Eigenfunctions of Symmetric Operators. *SIAM J. Numer. Anal.*, vol. 5, pp. 64–70.

Oudet, E. (2004): Numerical minimization of eigenmodes of a membrane with respect to the domain. *COCV*, vol. 10, pp. 315–330.

Troesch, B. A. (1973): Elliptical membranes with smallest second eigenvalue. *Math. Comp.*, vol. 27, pp. 767–772.